HHS Public Access

Author manuscript

Biochemistry. Author manuscript; available in PMC 2021 August 06.

Published in final edited form as:

Biochemistry. 2015 December 08; 54(48): 7098–7109. doi:10.1021/acs.biochem.5b00994.

H-NOX from *Clostridium botulinum*, like H-NOX from *Thermoanaerobacter tengcongensis*, Binds Oxygen but with a Less Stable Oxyferrous Heme Intermediate

Gang Wu[*], **Wen Liu**[#], **Vladimir Berka**, **Ah-Lim Tsai**[*]

Division of Hematology, Department of Internal Medicine, The University of Texas–Medical School at Houston, 6431 Fannin Street, Houston, Texas 77030, United States

Abstract

Heme nitric oxide/oxygen binding protein isolated from the obligate anaerobe *Clostridium botulinum* (*Cb* H-NOX) was previously reported to bind NO with a femtomolar K_D (Nioche, P. et al. *Science* 2004, *306*, 1550–1553). On the other hand, no oxyferrous *Cb* H-NOX was observed despite full conservation of the key residues that stabilize the oxyferrous complex in the H-NOX from *Thermoanaerobacter tengcongensis* (*Tt* H-NOX) (the same study). In this study, we re-measured the kinetics/affinities of *Cb* H-NOX for CO, NO, and O_2. K_D(CO) for the simple one-step equilibrium binding was 1.6×10^{-7} M. The K_D(NO) of *Cb* H-NOX was 8.0×10^{-11} M for the first six-coordinate NO complex, and the previous femtomolar K_D(NO) was actually an apparent K_D for its multiple-step NO binding. An oxyferrous *Cb* H-NOX was clearly observed with a $K_D(O_2)$ of 5.3×10^{-5} M, which is significantly higher than *Tt* H-NOX's $K_D(O_2) = 4.4 \times 10^{-8}$ M. The gaseous ligand binding of *Cb* H-NOX provides another supportive example for the "sliding scale rule" hypothesis (Tsai, A.-L. et al. *Antioxid. Redox Signal.* 2012, *17*, 1246–1263), and the presence of hydrogen bond donor Tyr139 in *Cb* H-NOX selectively enhanced its affinity for oxygen.

Graphical Abstract

[*]**Corresponding Authors**: (G.W.) Address: Hematology Division, Department of Internal Medicine, The University of Texas–Medical School at Houston, 6431 Fannin Street, Houston, TX 77030; phone, (713)-500-6802; fax, (713)-500-6812; gang.wu@uth.tmc.edu. (A.-L.T.) phone, (713)-500-6771; fax, (713)-500-6812; ah-lim.tsai@uth.tmc.edu.

[#]**Present Address**: Center for Infectious and Inflammatory Diseases, Texas A&M University - Health Science Center, 2121 West Holcombe Blvd, Houston, TX 77030.

Supporting Information

The Supporting Information is available free of charge on the ACS Publications website at DOI: 10.1021/acs.biochem.5b00994. (1) CO and NO binding parameters of Y140F *Tt* H-NOX (Table S1); (2) binding of CO to wt *Cb* H-NOX (Figure S1); (3) binding of CO to Y139F *Cb* H-NOX (Figure S2); (4) computer fitting of the NO binding to the 6c NO-heme-His complex in *Cb* H-NOX (Figure S3); (5) kinetics of the formation/dissociation of O_2 complex of *Tt* H-NOX (Figure S4); and (6) optical spectra of resting wt *Cb* and *Tt* H-NOXs (Figure S5) (PDF)

The authors declare no competing financial interest.

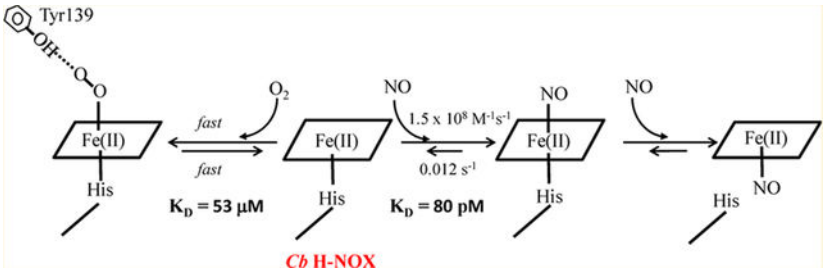

Heme nitric oxide/oxygen binding proteins (H-NOXs) are a family of bacterial hemoproteins, identified based on their significant sequence homology with the heme domain [β1(1–194)] of the only mammalian heme NO receptor soluble guanylyl cyclase (sGC).[1,2] In bacterial genome, H-NOX proteins are either encoded in the same operon with putative histidine kinases or diguanylate cyclases, or are domains of methyl-accepting chemotaxis proteins (MCP). As sGC, all H-NOX proteins conspicuously bind nitric oxide (NO) and carbon monoxide (CO).[3] On the other hand, H-NOXs isolated from different organisms exhibit a drastic difference in O_2 binding.[4] sGC and H-NOXs from facultative anaerobes, such as the one found in *Vibrio cholera* (*Vc* H-NOX),[5] reacts with O_2 but does not form a stable oxyferrous complex, while H-NOXs from obligate anaerobes, like the one found in *Thermoanaerobacter tengcongensis* (*Tt* H-NOX), bind O_2 with strong affinities and form stable oxyferrous complexes. The binding of O_2 to H-NOXs in obligate anaerobes may provide these organisms a mechanism to sense O_2 for self-defense. In obligate anaerobe *Clostridium botulinum* (*C. botulinum*), genome screening identifies a two-domain protein with an N-terminal H-NOX domain (*Cb* H-NOX or CB-SONO$_{HD}$) and a C-terminal MCP domain.[6] *Cb* H-NOX has been reported to bind NO with a femtomolar dissociation constant, K_D, much smaller than those of other H-NOXs; however, no oxyferrous *Cb* H-NOX was observed despite conservation of all the key residues which stabilize oxyferrous *Tt* H-NOX.[6,7]

All the H-NOXs and sGC possess a 5-coordinate (5c) heme with a proximal neutral histidine ligand (5c heme-His), as shown by structural determination[6–10] or sequence homology comparison. Although the 5c histidine-ligated ferrous hemoproteins with different structural folds bind NO, CO, and O_2 with different K_D's, covering a dynamic range up to 9 orders for each gaseous ligand, bioinformatics analysis reveals a simple "sliding scale rule" relationship between individual log K_D sets of each hemoprotein.[3,11] This hypothetic "sliding scale rule" states that for a 5c neutral histidine-ligated ferrous hemoprotein (or model compound), its log K_D(NO), log K_D(CO), and log K_D(O_2) fall on an approximately straight line in the plot of log K_D's versus ligand type, and the difference in the immediate protein environments around the heme cause a vertical parallel shift of such lines for each hemoprotein (or model compound) into a 9-order dispersion.[3,11] The "sliding scale rule" has been examined against many hemoproteins, including sGC and H-NOX from *Nostoc punctiforme* (*Ns* H-NOX), and heme model compound, such as PPIX(1-MeIm).[11,12] A recent example is *Vc* H-NOX, whose binding to the gaseous ligands is shown to also follow the "sliding scale rule".[5] Hemoproteins' parallel pattern of log K_D(NO)-log K_D(CO)-log K_D(O_2) lines described in the "sliding scale rule" has been ascribed to three major factors, including the presence of a proximal neutral histidine ligand, direct distal steric hindrance,

and proximal constraints for in-plane iron movement. This hypothetical rule provides an empirical tool to predict the affinities of a hemoprotein to any two of NO, CO, and O_2 based on its measured affinity for the third one.[3,11] On the other hand, deviations from the "sliding scale rule" are observed in some hemoproteins with a neutral histidine-ligated heme, and their log K_D(NO)'s and/or log $K_D(O_2)$'s are significantly lower than the values predicted by parallel linear projection going through their observed log K_D(CO)'s. These deviations are due to mechanisms which further stabilize the NO-heme and/or O_2-heme complexes of these hemoproteins. The deviation of K_D(NO)'s from the parallel linear pattern in some of these hemoproteins is attributed to the multiple steps in their NO bindings. In these hemoproteins, NO binding to heme first generates a 6-coordinate (6c) NO-heme-His complex, which later converts to a 5c NO-heme complex due to dissociation of the proximal histidine. Apparent affinity $K_{D,apparent}$(NO), as the ratio between the off-rate of the final stable 5c NO-heme complex, k_{off}(5c), and the on-rate of the initial 6c NO-heme-His complex, k_{on}(6c), is much lower than the K_D(NO) of the initial 6c NO-heme-His complex, $K_D(NO)(6c) = k_{off}(6c)/k_{on}(6c)$. A good example of multistep NO binding is found in sGC, whose $K_{D,apparent}$(NO) is ~3 orders lower than its $K_D(NO)(6c)$, which agrees perfectly with the "sliding scale rule".[3] Enhancement of O_2 affinity (lower $K_D(O_2)$) is usually observed in hemoproteins with a distal hydrogen-bond donor(s). For example, the presence of H64 in myoglobin and Y140 in *Tt* H-NOX results in $K_D(O_2)$'s much smaller than the predicted values based on linear extrapolation from their log K_D(NO)-log K_D(CO) lines.[11] *Cb* H-NOX, with its reported extremely low K_D(NO) but no detectable O_2 binding, even with retaining of all key residues in stabilizing oxyferrous complex in *Tt* H-NOX,[6] appears to be an outlier to the "sliding scale rule".

In this study, we re-assessed the gaseous ligand binding of *Cb* H-NOX in an effort to clarify two important issues. First, the reported femtomolar K_D(NO), 3.0×10^{-14} M, for *Cb* H-NOX is an apparent value;[6] what is then the $K_D(NO)(6c)$ for *Cb* H-NOX? Second, is oxyferrous complex intermediate in *Cb* H-NOX observable? To define the $K_D(NO)(6c)$ of *Cb* H-NOX, we measured the k_{on}(NO) and k_{off}(NO) of its 6c NO-heme-His complex. This study demonstrates that logarithms of $K_D(NO)(6c)$ and K_D(CO) in wt or Y139F *Cb* H-NOXs agree well with the "sliding scale rule". Moreover, wild type *Cb* H-NOX is shown to bind O_2 and form an oxyferrous complex, but its $K_D(O_2)$ is three orders higher than that of *Tt* H-NOX. As a comparison, we also measured the kinetics and affinities of NO, CO, and O_2 to wt *Tt* H-NOX; a complete set of parameters of gaseous ligand binding has so far not been available for *Tt* H-NOX. The affinities of wt *Tt* H-NOX for NO and CO also follow the "sliding scale rule". Deviations of $K_D(O_2)$'s of *Cb* and *Tt* H-NOXs from the "sliding scale rule" are ascribed to the stabilizing hydrogen bonding of distal Y139 in *Cb* and Y140 in *Tt* H-NOX, respectively.

MATERIALS AND METHODS

Materials.

Carbon monoxide (CO) and nitric oxide (NO) gases were from Matheson-TriGas Inc. (Houston, TX). NO was prepurified by passing through a NaOH trap to remove nitrous and nitric acid contaminants. Sodium hydrosulfite ($Na_2S_2O_4$), imidazole, heme, δ-

aminolevulinic acid, isopropyl-1-thio-β-D-galactopyranoside, ampicillin, kanamycin, chloramphenicol, and egg lysozyme were from Sigma (St. Louis, MO). Restriction enzymes and other DNA modifying enzymes were purchased from New England BioLabs (Beverly, MA). Oligonucleotides were obtained from Integrated DNA Technologies (Coralville, IA). Reagents for DNA extraction and purification were from Qiagen (Valencia, CA). Immunoblotting reagents were from Bio-Rad (Hercules, CA). Plasmid vectors pET43.1a and pET28b, and *Escherichia coli* strains Rosetta 2(DE3)pLysS and Rosetta-gami B(DE3), and anti-HisTag monoclonal antibody were from Novagen (Madison, WI). TALON metal affinity resin was purchased from BD Biosciences Clontech (Palo Alto, CA). Other chemicals were all of reagent grade.

Construction of the Expression Vectors for H-NOXs.

The cDNA of wt *Cb* H-NOX from *C. botulinum* A strain (ATCC3502) was synthesized with the gene sequence optimized for *E. coli* codon usage, replacing several rare codons with high-frequency synonymous codons. The cDNA contained the codons for six histidines at the N-terminus. The cDNA was cloned into pBSK vector (Epoch LifeScience, Houston, TX) and amplified. The wt *Cb* H-NOX cDNA was then released by digesting with *Nco*I and *Xho*I, and subcloned into pET28b vector. The integrity of the resulting plasmid was confirmed by restriction digestion and DNA sequencing (Lone Star Labs, Houston, TX).

Y139F point mutation in *Cb* H-NOX was introduced using the QuikChange Site-directed Mutagenesis kit (Stratagene, La Jolla, CA). The mutagenic primer (base changes are underlined), 5′-CGCGGCATGTTTGATTTTTTCTGGGCCTGCTG-3′, together with its complementary (antisense) strand, 5′-CAGCAGGCCCAGAAAAAAATCAAACATGCCGCG-3′, were used in a PfuUltra polymerase-initiated reaction, using wt *Cb* H-NOX in pET28b vector as the template. The DNA template of wt *Cb* H-NOX was then removed by digestion with *Dpn*I, and the cDNA of Y139F *Cb* H-NOX was transformed into *E. coli* XL-10 competent cells. The mutation was verified by DNA sequencing.

The sequence of wt *Tt* H-NOX MB4 gene was first optimized for *E. coli* codon usage by replacing several rare codons with high-frequency synonymous codons. This optimized cDNA contained six histidine codons inserted upstream of the stop codon. The cDNA was amplified in pBSK vector and then subcloned into pET43.1a vector. The integrity of the resulting plasmid was confirmed by restriction digestion and DNA sequencing.

Y140F point mutation in *Tt* H-NOX was introduced using the QuikChange Site-directed Mutagenesis kit (Stratagene, La Jolla, CA). The mutagenic primer (base changes are underlined), 5′-CGCAAGATGTACGATTTCTTTCTGGGCCTGATC-3′, together with its complementary (antisense) strand, 5′-GATCAGGCCCAGAAAGAAATCGTACATCTTGCG-3′, were used in a PfuUltra polymerase-initiated reaction, using wt *Tt* H-NOX in pET43.1a vector as the template. The DNA template of wt *Tt* H-NOX was then removed by digestion with *Dpn*I, and the cDNA of Y140F *Tt* H-NOX was transformed into *E. coli* XL-10 competent cells. The mutation was verified by DNA sequencing.

Expression and Purification of H-NOXs.

The wild type *Cb* and *Tt* H-NOXs and their point mutants were expressed and purified following the similar procedure as described previously[5] and are summarized briefly as follows. The H-NOXs were overexpressed in *E. coli* Rosetta 2(DE3)pLysS strain (for wt and Y139F *Cb* H-NOXs) or Rosetta-gami B(DE3) strain (for wt and Y140F *Tt* H-NOXs). The cells were first grown at 37 °C in Terrific Broth medium containing chloramphenicol and kanamycin until A_{610} reached 0.8. Then heme, δ-aminolevulinic acid, and isopropyl-1-thio-β-D-galactopyranoside were added to the culture, and the cells were grown at 20 °C for another 48 h before harvest.

Cells harvested above were lysed by sonication in 100 mM potassium phosphate, pH 7.5 containing 100 mM NaCl, 10% (v/v) glycerol and egg lysozyme (3.0 mg/mL). Supernatant after centrifugation at 100,000*g* was loaded onto TALON affinity resin, and the H-NOXs were eluted with the same buffer (without lysozyme) containing 250 mM imidazole. The purities of the H-NOXs were typically ≥95%, checked with SDS-PAGE (data not shown).

Stopped-Flow Experiments.

The association and dissociation kinetics of NO, CO, and O_2 to anaerobic ferrous H-NOXs were studied with an Applied Photophysics (Leather-head, UK) model SX-18MV stopped-flow instrument, and optically following the absorbance changes at different wavelengths with a monochromator or the whole spectral changes with a diode-array accessory. The sample handling unit was kept in an anaerobic chamber (COY Lab Products, Inc., Grass Lake, MI). Ferrous H-NOXs used in all the experiments were prepared by $Na_2S_2O_4$ titration after five alternating cycles of vacuum and argon displacement in a tonometer. No extra $Na_2S_2O_4$ existed in the final samples judged by the absence of the absorbance due to $Na_2S_2O_4$. Rapid scan data was analyzed with the global analysis method using the Pro-Kineticist package by Applied Photophysics. Observed rate constants, k_{obs}, of single wavelength data under pseudo-first order conditions were obtained by fitting the time courses of optical changes to the standard exponential function:

$$A = A_f + ae^{-k_{obs}t} \quad (1)$$

where A_f, t, and a are the final optical absorbance, reaction time, and amplitude of optical change, respectively. Second-order association rate constant k_{on} was derived from the slope in the secondary plots of k_{obs} versus gaseous ligand concentration [L]:

$$k_{obs} = k_{on} \times [L] + k_{off} \quad (2)$$

The *y*-intercept corresponds to k_{off}. However, in this study, k_{off} constants for the NO and CO complexes are small, and fitting errors prevent extracting their accurate values based on the *y*-intercepts of the secondary plots. Dissociation constants were therefore determined using competition methods as explained in Results.

When measuring the formation rate of a 6c NO-heme-His complex in a H-NOX, the protein was mixed with an equal concentration of NO, and the k_{obs} was obtained by fitting the time course to the equation of a second-order reaction:

$$A = A_f + A_0/(A_0 \times k_{obs} \times t + 1) \quad (3)$$

where A_0 is the initial optical absorbance and t is the reaction time. Second order rate constant in unit of M^{-1} s^{-1} was obtained by multiplying k_{obs} with the difference extinction coefficient, $\Delta\varepsilon$.

EPR Spectroscopy.

EPR spectra were recorded on a Bruker EMX spectrometer. Data analyses and spectral simulations were conducted using WinEPR and SimFonia programs furnished with the EMX system. EPR at 115 K was conducted using the following parameters: frequency, 9.29 GHz; modulation frequency, 100 kHz; modulation amplitude, 2.0 G; and time constant, 0.33 s.

EPR samples of NO complexes were prepared by injecting desired volumes of 2 mM NO stock into ferrous H-NOXs inside EPR tubes and the reactants were then mixed. The procedures were conducted inside the anaerobic chamber, and then the EPR tubes were transferred outside and quickly frozen in an ethanol/dry ice mixture. The times between NO injection and sample freezing were less than 1 min.

Computer Modeling.

Time courses of A_{422} during the reactions between 2.3 μM ferrous *Cb* H-NOX with varied levels of NO, 25 μM, 0.1 mM, 0.2 mM, 0.3 mM, 0.4 mM, 0.5 mM, 0.65 mM, 0.8 mM, and 1 mM were fitted simultaneously using SCoP Program (Simulation Resources Inc., Redlands, CA). The model used for the fitting was based on reactions I and II (Scheme 1, $C \Leftrightarrow D \Leftrightarrow E$). Parameters including the extinction coefficients for both 6c NO-heme-His and 5c NO-heme complexes and rate constant k_2 were set to their experimentally measured values. Other kinetic parameters including rate constants k_1, k_{-1}, and k_{-2} and the extinction coefficient for the putative transient quaternary complex were allowed to float, but initial value for k_{-2} was ~0, and the ratio of k_{-1}/k_1 was equal to K_D, determined by experiment. The global minimum of the error surface during the nonlinear regression for the multiple time courses was located by a “principal axis method” algorithm (PRAXIS), which is capable of random jumping out of local minima to find the global minimum.[13] The goodness of fit was evaluated by “least squares” method, which was calculated as follows,

$$E = \sqrt{\left(\sum_{k=1}^{n} (fk - yk)^2\right)/n} \quad (4)$$

where E represents the error function, n is the number of data point in each experimental time course, and f_k and y_k are the fitted and experimental values at each time point, respectively. A good fit was indicated by its small value of E.

RESULTS

Kinetics of CO Binding to Ferrous *Cb* and *Tt* H-NOXs.

CO binding to *Cb* H-NOX was first characterized in this study since it was not reported before; and among NO, CO, and O_2 ligands, the kinetics of CO binding to hemoproteins is the simplest. CO bound ferrous wt *Cb* H-NOX in a simple reversible one-step reaction (Scheme 1, $A \Leftrightarrow B$) which shifted the Soret peak from 431 to 424 nm with no spectral intermediate (Figure S1A). Observed rate constants, k_{obs}, obtained by fitting the time courses at 424 nm exhibited a linear dependence on [CO] (Figure S1B) and the second-order association rate constant equals the slope, $k_{on}(CO) = 1.5 \times 10^6\ M^{-1}\ s^{-1}$ (Figure S1B, inset and Table 1). The dissociation rate constant, k_{off}, was measured with the NO displacement method[14] by reacting CO-heme complex with 1 mM NO (Figure S1C). The $k_{off}(CO)$ of wt *Cb* H-NOX thus determined was $1.0\ s^{-1}$ (Table 1). The equilibrium dissociation constant, $K_D(CO)$ for wt *Cb* H-NOX, was calculated to be 6.7×10^{-7} M (Table 1).

The CO binding kinetics to ferrous Y139F *Cb* H-NOX was similar to that of wt *Cb* H-NOX (Figure S2). Binding of CO to ferrous Y139F *Cb* H-NOX shifted the Soret peak from 432 to 424 nm in a single step reaction (Figure S2A). The $k_{on}(CO)$ of Y139F *Cb* H-NOX is slightly faster than that of wt *Cb* H-NOX, $k_{on}(CO) = 3.4 \times 10^6\ M^{-1}\ s^{-1}$ (Figure S2B, inset and Table 1). The dissociation rate constant of Y139F *Cb* H-NOX CO-heme complex, $k_{off}(CO) = 1.1\ s^{-1}$ (Figure S2C and Table 1), is the same as that of wt *Cb* H-NOX CO-heme complex. The equilibrium constant of Y139F *Cb* H-NOX for CO, $K_D(CO)$ was calculated as 3.3×10^{-7} M (Table 1). Y139F *Cb* H-NOX binds CO with slightly higher affinity than wt *Cb* H-NOX.

The kinetics for CO binding to wt *Tt* H-NOX were similarly measured (data not shown), $k_{on}(CO) = 3.3 \times 10^6\ M^{-1}\ s^{-1}$ and $k_{off}(CO) = 0.5\ s^{-1}$ (Table 1). The $k_{on}(CO)$ is quite similar to published values, either with laser photolysis or stopped-flow methods.[15] On the other hand, $k_{off}(CO)$ measured in this study is about 7-fold lower than the published values.[15] The reason for this discrepancy is unclear since similar NO displacement method was used in both studies.[15] In this study, wt *Tt* H-NOX is measured to bind CO slightly more tightly than wt *Cb* H-NOX with a $K_D(CO) = 1.6 \times 10^{-7}$ M (Table 1).

Binding of NO to Ferrous *Cb* and *Tt* H-NOXs.

To characterize the binding of NO to *Cb* H-NOX, a rapid-scan stopped-flow method was used to follow the optical changes during the reactions of ferrous *Cb* H-NOX with either stoichiometric (Figure 1A) or excess NO (10 equiv, Figure 1C). Ferrous wt *Cb* H-NOX bound stoichiometric NO promptly with most of the reaction lost in the dead time of the stopped-flow apparatus, indicating a very large $k_{on}(NO)$ (Figure 1A). The Soret peak shifted from 431 to 420 nm with isosbestic points at 424 and 455 nm (Figure 1A). The wavelength of the product indicates the formation of a typical 6c NO-heme-His complex (Figure 1A, inset, A → B). The conformation of the 6c NO-heme-His complex then began to change indicated by the decay of the Soret peak (Figure 1A, inset, B → C). In a longer reaction time, the Soret peak further decayed and shifted to 409 nm (Figure 1A), indicating breakage of Fe-His bond in the initial 6c NO-heme-His complex and conversion to a 5c NO-heme complex. When reacted with 10 equiv NO, a 6c NO-heme-His complex formed in the dead

time of the stopped-flow apparatus as indicated by the first captured spectrum (1.28 ms after mixing) which exhibited an absorption maximum at 420 nm (Figure 1C). The observed optical change was a monophasic shift to 407 nm (Figure 1C), indicating conversion to a 5c NO-heme complex. However, the conversion was likely incomplete since a pure 5c NO-heme complex usually exhibits a Soret peak at wavelength ≤400 nm in many hemoproteins including H-NOXs and sGC.[5,12,16,17]

The optical change during the reaction of ferrous Y139F *Cb* H-NOX with stoichiometric NO (Figure 1B) was similar to that of wt *Cb* H-NOX (Figure 1A), the Soret peak shifted from 432 to 420 nm with isosbestic points at 423 and 457 nm (Figure 1B), indicating the formation of a 6c NO-heme-His complex (Figure 1B, inset, A → B). Most of the optical change was lost in the dead time of the stopped-flow apparatus, indicating a very fast binding of NO to Y139F *Cb* H-NOX. The conformation of the 6c NO-heme-His complex then began to change, indicated by the decay of the Soret peak (Figure 1B, inset, B → C). However, different from the case in wt *Cb* H-NOX, the Soret peak further decayed slightly without further shift in wavelength even after much longer reaction time (Figure 1B), indicating that the initial 6c NO-heme-His complex in Y139F *Cb* H-NOX underwent certain conformational change(s) without dissociation of the proximal histidine ligand. In the reaction of Y139F *Cb* H-NOX with excess NO, a 6c NO-heme-His complex formed in the dead time of the stopped-flow apparatus, and the first spectrum captured at 1.28 ms exhibited an absorption peak at 420 nm (Figure 1D). However, in contrast to that in wt *Cb* H-NOX (Figure 1B), the Soret peak of the 6c NO-heme-His complex formed in Y139F *Cb* H-NOX with excess NO decayed monophasically without shift in wavelength (Figure 1D), indicating that certain conformational change(s) happened without dissociation of the proximal histidine ligand. In line with that observed previously, the Fe-His bond between heme and the proximal histidine in the 6c NO-heme-His complex of *Cb* H-NOX is stabilized by the Y139 to phenylalanine mutation.[6]

To determine the large formation rates of the 6c NO-heme-His complexes in wt and Y139F *Cb* H-NOXs, k_{on}(NO), we measured the kinetics under true second-order conditions, using a [NO]:[*Cb* H-NOX] ratio of 1:1 as described before (Figure 2A,C).[5,11] The time courses at 430 nm (wt *Cb* H-NOX) or 432 nm (Y139F *Cb* H-NOX) were fitted to a second-order, irreversible mechanism (eq 3, Figure 2A,C). The formation rate constants of 6c NO-heme-His complexes were obtained as $k_{on}(NO) = k_{obs} \times \Delta\varepsilon$ and $\Delta\varepsilon_{430\ nm} = 37\ mM^{-1}\ cm^{-1}$ for wt *Cb* H-NOX (Figure 1A), while $\Delta\varepsilon_{432\ nm} = 39.2\ mM^{-1}\ cm^{-1}$ for Y139F *Cb* H-NOX (Figure 1C). The k_{on}(NO) was $1.5 \times 10^8\ M^{-1}\ s^{-1}$ for wt *Cb* H-NOX (Table 1), similar to the value estimated previously for *Cb* H-NOX based on diffusion limitation assumption.[6] Y139F *Cb* H-NOX had a slightly slower k_{on}(NO), $4.3 \times 10^7\ M^{-1}\ s^{-1}$ (Table 1).

The dissociation rate constants of the 6c NO-heme-His complexes in both wt and Y139F *Cb* H-NOXs, k_{off}(NO), were measured using the sequential stopped-flow method.[5,11] The 6c NO-heme-His complexes were generated by reacting either wt or Y139F *Cb* H-NOX with stoichiometric NO, aged for 100 ms, and then reacted with 0.5 mM CO in 25 mM $Na_2S_2O_4$ to displace and consume the dissociated NO, respectively.[5,11] Exponential increase in A_{424} was observed following the second mixing (Figure 2B,D), indicating the formation of CO-heme complex. Fitting the time courses at 424 nm to the single-exponential function (eq 1)

yielded a dissociation rate constant k_{off}(NO) of 0.012 s^{-1} for the 6c NO-heme-His in wt *Cb* H-NOX and a slightly slower rate of 5.0×10^{-3} s^{-1} for the same complex in Y139F *Cb* H-NOX (Table 1). The k_{off}(NO) are much slower than k_{on}(CO) of wt or Y139F *Cb* H-NOXs (Table 1), in line with the rate of NO displacement by CO being limited by the NO dissociation from the 6c NO-heme-His complexes. The K_D(NO)(6c)'s, calculated as the ratio of k_{off}(NO)/k_{on}(NO), were 8.0×10^{-11} M and 1.2×10^{-10} M for wt and Y139F *Cb* H-NOXs, respectively (Table 1). The reaction to form 6c NO-heme-His complex in *Cb* H-NOX is represented in Scheme 1 ($A \Leftrightarrow C$).

In the presence of excess NO, the 6c NO-heme-His complex in wt *Cb* H-NOX converted to a 5c NO-heme complex (Scheme 1, *E*), and the kinetics of this process was studied under pseudo first-order conditions, following the time courses of A_{422} (Figure 3). Formation of 6c NO-heme-His (Scheme 1, *C*) complex was complete within the dead time of the stopped-flow apparatus, and the k_{obs}'s are the rate constants for its further conversion to the 5c NO-heme complex (Figure S3). The k_{obs}'s increased with [NO] and gradually leveled off at high [NO] (Figure 3, inset). This pattern of [NO]-dependence of k_{obs} suggests (1) in the presence of excess NO, conversion to the 5c NO-heme complex presumably proceeds through a quaternary complex, NO-heme--NO(--His) (Scheme 1, *D*), formed by the reaction of 6c NO-heme-His complex with NO at the proximal side of heme (Scheme 1, $C \Leftrightarrow D$) and thus shows [NO]-dependence of k_{obs}; (2) conversion from the hypothetic quaternary complex to the 5c NO-heme complex (Scheme 1, $D \Leftrightarrow E$) becomes rate-limiting at high [NO]. The formation of 5c NO-heme complex in wt *Cb* H-NOX with excess NO can be represented with reactions I and II:

$$\text{6c NO-heme-His} + \text{NO} \Leftrightarrow \text{NO-heme--NO (--His)}(k_1, k_{-1}) \quad \text{(I)}$$

$$\text{NO-heme--NO(--His)} \Leftrightarrow \text{5c NO-heme} + \text{NO}(k_2, k_{-2}) \quad \text{(II)}$$

At low [NO], the first step is rate-limiting and the k_{obs} increases with [NO], while at high [NO], the second step becomes rate-limiting and the k_{obs} levels off. The [NO]-dependence of k_{obs} can be described using the following hyperbolic function:

$$k_{obs} = k_2 \times [\text{NO}]/(K_D + [\text{NO}]) + k_{-2} \quad (5)$$

Here the reassociation rate constant of NO with 5c NO-heme to form NO-heme--NO(--His) complex, k_{-2}, is small and can be ignored. The k_2 was estimated ~790 s^{-1} and $K_D \approx 570$ μM based on eq 5 (Figure 3, inset). Such a saturating behavior in the [NO]-dependence of 5c NO-heme formation kinetics was also observed for *Vc* H-NOX[5] but not for sGC[18] or *Ns* H-NOX.[12] In fact the maximum formation rates for the 5c NO-heme complex are quite similar for *Cb* and *Vc* H-NOXs.[5] A computer model was built based on reactions I and II to fit the time courses during the formation of the 5c NO-heme complex in *Cb* H-NOX. The values for k_1 and k_{-1} obtained by simultaneous fitting to kinetic data obtained at nine different [NO] were 1.8×10^7 M^{-1} s^{-1} and 2.0×10^4 s^{-1}, respectively (Figure S3). Although both k_1 and k_{-1} were allowed to float during the fitting, K_D = 1.1 mM of reaction I, calculated from the fitted values of k_1 and k_{-1}, agrees reasonably well with the experimentally measured

value (Figure 3, inset). According to the mechanism, the hypothetic quaternary complex has the best chance accumulating enough for observation at high [NO]. However, at the highest [NO] available (1 mM), the Soret peak of the spectrum captured at the shortest reaction time (1.28 ms) was at 420 nm, the same as that observed at much lower [NO] and the subsequent spectral change exhibited a single one step shift to 407 nm (data not shown). Therefore, at the highest [NO], no spectral feature attributed to the predicted transient quaternary complex could be resolved in addition to the initial 6c and final 5c NO-heme complexes. The transient nature of the quaternary complex is due to the very large dissociation rate constant k_{off} of the quaternary complex, 2×10^4 s^{-1} (Scheme 1, $D \rightarrow C$). Moreover, the equilibrium constant, $K_D = k_{off}/k_{on}$, between the 6c NO-heme-His complex and the quaternary complex NO-heme--NO(--His) complex, can be estimated to reach 1.1 at the highest [NO] available. This large K_D led to the incomplete conversion from the 6c NO-heme-His complex to the 5c NO-heme complex (Scheme 1, $C \rightarrow E$), although the conversion from the quaternary complex to the 5c complex is essentially irreversible (Scheme 1, $D \Leftrightarrow E$).

The dissociation rate constants of the 5c NO-heme complex in wt *Cb* H-NOX, k_{off}(5c) (Scheme 1, $E \rightarrow A$), were measured by reacting the 5c NO-heme complex with 0.5 mM CO in 25 mM $Na_2S_2O_4$ (data not shown). The 5c NO-heme exhibited a biphasic NO dissociation kinetics, with rates of 1.1×10^{-2} s^{-1} (45% total amplitude change) and 1.1×10^{-3} s^{-1} (55% total amplitude change) (Table 1). The rate of the fast phase of NO dissociation is essentially the same as the k_{off}(NO) of its 6c NO-heme-His complex (Figure 2B) which did not fully transform to 5c NO-heme complex. The slow phase thus represents the NO dissociation from the 5c NO-heme complex in wt *Cb* H-NOX at a rate 10 times slower than from the corresponding 6c NO-heme-His complex (Table 1). The kinetic events during the NO binding to *Cb* H-NOX are summarized in Scheme 1 ($A \rightarrow E$).

The association/dissociation rate constants for the 6c NO-heme-His complex in *Tt* H-NOX were measured using the same method as for *Cb* H-NOX, and we obtained k_{on}(NO) = 1.5×10^8 M^{-1} s^{-1} and k_{off}(NO) = 3.4×10^{-3} s^{-1} (Table 1). Although the k_{off}(NO) of wt *Tt* H-NOX was measured before using similar method,[19] it is 6-fold lower than that measured in this study. The reason for the discrepancy is not clear yet. Compared to the kinetic parameters of NO binding in *Cb* H-NOX, k_{on}(NO) of the 6c NO-heme-His complex in wt *Tt* H-NOX is the same as in wt *Cb* H-NOX, but k_{off}(NO) in wt *Tt* H-NOX is very similar to that in Y139F *Cb* H-NOX (Table 1). The K_D(NO) of the 6c NO-heme-His complex in wt *Tt* H-NOX, 2.3×10^{-11} M, a little lower than that of the corresponding 6c NO-heme-His complex in *Cb* H-NOX (Table 1).

EPR of NO Complexes in *Cb* and *Tt* H-NOXs.

Spectroscopic studies indicate that distal tyrosine modulates the strength of the Fe-His bond in the 6c NO-heme-His complex in *Cb* H-NOX but not in *Tt* H-NOX.[6,20] In this study, the NO-heme complexes formed in these H-NOXs were studied more in detail using EPR. In the presence of excess NO, the EPR spectrum of NO-heme complex in wt *Cb* H-NOX majorly exhibited features typical for a 5c NO-heme complex (Figure 4a), confirming breakage of the Fe–His bond in the initial 6c NO-heme-His complex, in line with the shift of absorption peak from 420 to 407 nm during the reaction of wt *Cb* H-NOX with excess NO (Figure 1C,

and previously[6]). On the other hand, the small EPR feature at $g = 1.978$ indicated the existence of a minor portion of a 6c NO-heme-His complex (Figure 4a). The 6c NO-heme-His complex accounted for ~30% of total [spin] against a standard EPR spectrum of a pure 5c NO-heme complex (Figure 4c) obtained by subtracting 30% of a simulated 6c NO-heme-His EPR spectrum (Figure 4b) from spectrum 4a. EPR therefore demonstrates an incomplete conversion from the initial 6c NO-heme-His complex to 5c NO complex in wt *Cb* H-NOX, corroborating the observed Soret peak at 407 nm (Figure 1C) not that for a pure 5c NO-heme complex (≤400 nm). On the other hand, percentage of 6c and 5c NO complexes estimated by EPR varied from that estimated based on optical kinetic data (30% vs 45%) and the discrepancy could be due to the very low measurement temperature of EPR samples.

In line with the optical data from this (Figure 1D) and previous studies,[6] EPR data demonstrated the modulation effect of Y139F mutation on the stability of the Fe-His bond in the 6c NO-heme-His complex as significantly more EPR features due to a 6c NO-heme-His complex were observed in the reaction of Y139F *Cb* H-NOX with excess NO (Figure 4d). Some 6c NO-heme-His complex did convert to a 5c NO-heme complex in the 1 min reaction as indicated by the three-line hyperfine features observed at $g = 2.009$, which is typical of a 5c NO-heme complex (Figure 4d). About 30% 6c NO-heme-His was estimated to have converted, as indicated by the EPR of a nearly pure 6c NO-heme-His complex (Figure 4f) obtained by subtracting ~30% of a simulated 5c NO-heme EPR spectrum (Figure 4e) from spectrum 4d. Since optical data did not indicate significant conversion from 6c NO-heme-His complex to 5c NO-heme complex during the reaction of Y139F *Cb* H-NOX with excess NO (Figure 1D), the observed EPR features of a 5c NO-heme complex may be also introduced by the freezing of the EPR samples.

On the contrary to *Cb* H-NOX, optical data indicated that the corresponding Y140F mutation in *Tt* H-NOX does not change the coordination number of the NO complex, a 6c NO-heme-His complex is stable in both wt and Y140F *Tt* H-NOXs.[20] With excess NO, both wt and Y140F *Tt* H-NOXs, EPR signatures typical of a 6c NO-heme-His complex were observed (Figure 5A,C), and the EPR spectra were nicely simulated as 6c NO-heme-His complexes (Figure 5B,D). Both sets of hyperfine splitting constants resulted from the NO nitrogen (A_{N1}) and that from superhyperfine splitting from imidazole nitrogen (A_{N2}) are similar: 24G/7G for wild type and 23.2G/6.7G for Y140F *Tt* H-NOX, respectively. Although the Fe–His bond stayed unbroken in both 6c NO-heme-His complexes, the EPR data demonstrated for the first time noticeably different lineshapes of the two 6c NO-heme-His complexes in wt and Y140F *Tt* H-NOXs (Figure 5). The most noticeable difference was the shift of g_x from 2.090 to 2.069 of the 6c NO-heme-His (Figure 5A/B to 5C/D), indicating decreased heme rhombicity of the Y140F NO-heme-His complex. In conclusion, in *Cb* H-NOX, mutation of distal Y139 to phenylalanine stabilizes the Fe–His bond in its 6c NO-heme-His complex, but in *Tt* H-NOX, the same mutation Y140F alters the geometry of heme without an obvious effect on the stability of Fe–His bond. The association/dissociation kinetics of Y140F *Tt* H-NOX for NO and CO was also measured in the same way as above and is similar to that of wt *Tt* H-NOX (Table S1).

Reaction of O_2 with Ferrous *Tt* and wt and Y139F *Cb* H-NOXs.

Tt H-NOX has been shown to bind O_2 tightly.[21] In this study, the association/dissociation kinetics of O_2 to *Tt* H-NOX was remeasured using another method and compared to the published values. The binding rate constant, $k_{on}(O_2)$, was determined under true second-order reaction conditions, reacting ferrous *Tt* H-NOX with 1 equiv O_2 and following the time course of A_{430} (Figure S4A). Using this method, the $k_{on}(O_2)$ for *Tt* H-NOX was measured as 4.3×10^7 M^{-1} s^{-1} (Table 1). The $k_{off}(O_2)$ from oxyferrous *Tt* H-NOX was measured by following the time course of A_{430}, mixing oxyferrous *Tt* H-NOX with 25 mM $Na_2S_2O_4$ using the latter to consume the dissociated O_2 (Figure S4B). The k_{obs} was 1.9 s^{-1} and showed no dependence on the concentration of $Na_2S_2O_4$ (data not shown), indicating that the rate-limiting step was O_2 dissociation and the k_{obs} was the true $k_{off}(O_2)$ of oxyferrous *Tt* H-NOX. The affinity of wt *Tt* H-NOX for O_2 was calculated as $K_D(O_2) = k_{off}(O_2)/k_{on}(O_2) = 4.4 \times 10^{-8}$ M (Table 1). The measured kinetic parameters and affinity of wt *Tt* H-NOX to O_2 in this study (Table 1) are all similar to the published values.[20,22]

When anaerobic wt *Cb* H-NOX was mixed with aerobic buffer, an oxyferrous complex formed immediately (Scheme 1, $A \Leftrightarrow F$) and the reaction finished in the dead time of the stopped-flow apparatus (Figure 6A). The first spectrum captured at 1.28 ms after mixing showed a Soret peak at 422 nm, and the absorption band at 564 nm of ferrous wt *Cb* H-NOX split into a α band at 583 nm and a β band at 549 nm, consistent with formation of an oxyferrous complex (Figure 6A). The method which enabled successful measurement of $k_{on}(O_2)$ for wt *Tt* H-NOX (see above) failed for wt *Cb* H-NOX, since most of the reaction finished within the dead time of the stopped-flow apparatus under similar experimental conditions, by mixing wt *Cb* H-NOX with even stoichiometric O_2. This was likely due to a very large $k_{obs} = k_{on}(O_2) + k_{off}(O_2)$, $\gg 600$ s^{-1}, of wt *Cb* H-NOX. Large $k_{off}(O_2)$ also prevented fitting accurately to the time course of reaction III based on eq 3.

$$Cb\text{H-NOX} + O_2 \Leftrightarrow Cb\text{H-NOX-}O_2(k_{on}, k_{off}) \quad \text{(III)}$$

Since reaction III reached equilibrium quickly, preventing measuring $k_{on}(O_2)$ and $k_{off}(O_2)$ accurately, the $K_D(O_2)$ of oxyferrous wt *Cb* H-NOX was measured in the stopped-flow by titrating wt *Cb* H-NOX with varying levels of O_2, and the decrease of A_{432}, due to the formation of oxyferrous complex (reaction III), versus $[O_2]$ was monitored (Figure 6B). The $K_D(O_2)$ of wt *Cb* H-NOX was obtained by fitting to the plot of A_{432} versus $[O_2]$ to the following equation:

$$\Delta A_{432} = (\Delta A_{432,\max} \times [O_2])/(K_D + [O_2]) \quad (6)$$

The affinity of wt *Cb* H-NOX for O_2 obtained by this method was $K_D(O_2) = 5.3 \times 10^{-5}$ M (Table 1). Compared to wt *Tt* H-NOX, wt *Cb* H-NOX binds O_2 about 1200 times more weakly. Nonetheless, an oxyferrous complex does form in *Cb* H-NOX under atmospheric O_2 pressure. If the $k_{on}(O_2)$ of wt *Cb* H-NOX is assumed similar to that of wt *Tt* H-NOX, $k_{off}(O_2)$ of wt *Cb* H-NOX can be estimated: $k_{off}(O_2) = K_D(O_2) \times k_{on}(O_2) = \sim 2500$ s^{-1}, providing an estimation for how fast reaction III reaches equilibrium (Scheme 1, $A \Leftrightarrow F$).

Mutating Y139 to phenylalanine excludes Y139F *Cb* H-NOX from binding O_2, as no formation of any oxyferrous complex was observed when anaerobic Y139F *Cb* H-NOX was reacted with O_2-saturated buffer, with a $[O_2]$ = 600 μM (Figure 6C). The same mutation in *Tt* H-NOX, Y140F, also abolishes the formation of any oxyferrous complex in Y140F *Tt* H-NOX.[23] Both ferrous wt and Y139F *Cb* H-NOXs auto-oxidized to ferric state after prolonged incubation with O_2, presumably through transient association with O_2 (data not shown).

DISCUSSION

When the logarithms of true K_D(NO), K_D(CO), and K_D(O_2) of *Cb* and *Tt* H-NOXs are plotted in "sliding scale plot", their log K_D(NO)-log K_D(CO) lines parallel with those of sGC, *Ns*, *Vc* H-NOXs and heme model compound (Figure 7). Therefore, K_D(NO) and K_D(CO) of both *Cb* and *Tt* HOXs obey the "sliding scale rule". On the other hand, compared to that of *Ns* H-NOX, the log K_D(CO)-log K_D(O_2) lines in both *Cb* and *Tt* H-NOXs deviate downward from the extensions of their log K_D(NO)-log K_D(CO) lines (Figure 7), reflecting their enhanced O_2 affinity. The measured K_D(O_2)'s of wt *Cb* and *Tt* H-NOXs, 5.3×10^{-5} M and 4.4×10^{-8} M, respectively, much lower than the values estimated by linear extrapolation from log K_D(NO) via log K_D(CO), ~5.3×10^{-3} M for *Cb* H-NOX and ~1.0×10^{-3} M for *Tt* H-NOX, respectively. The deviation of its K_D(O_2) in *Tt* H-NOX from the "sliding scale rule" has been attributed to the stabilization of its oxyferrous complexes by its distal hydrogen bonding networks.[3,11] Such a distal hydrogen bonding network likely exists in *Cb* H-NOX due to the conservation of the several key amino acid residues,[6] resulting in stabilized oxyferrous complex and enhanced affinity for O_2. Compared to the previous study on the gaseous ligand binding of *Cb* H-NOX,[6] two major differences are noticeable: (1) a much lower K_D(NO) was measured previously (Figure 7, dark yellow circle and dashed line) and (2) oxyferrous *Cb* H-NOX was observable and characterized in this study but not reported previously.[6] The possible reasons for these differences are discussed below.

NO Binding to *Cb* H-NOX.

To calculate the true K_D(NO) in *Cb* H-NOX, both k_{on}(NO) and k_{off}(NO) should be of the same chemical reaction, namely, those for 6c NO-heme-His complex formation (Scheme 1, $A \Leftrightarrow C$):

$$\text{5c heme-His} + \text{NO} \Leftrightarrow \text{6c NO-heme-His}(k_{on}, k_{off}) \quad \text{(IV)}$$

In the previous study, the k_{on}(NO) of ~10^8 M^{-1} s^{-1} was not determined experimentally but an estimated value based on the assumption of diffusion limitation.[6] This is a good assumption and confirmed by the k_{on}(NO) measured experimentally in this study (Table 1), and the k_{on}(NO) of *Cb* H-NOX is comparable to those of many other bacterial H-NOXs and hemoproteins.[5,6,11] The femtomolar binding of NO to *Cb* H-NOX measured previously,[6] 3.0×10^{-14} M which is several orders tighter than the K_D(NO)'s of other H-NOXs,[5,12] was majorly due to the very slow k_{off}(NO), measured by following the decay of the EPR signal of a 5c NO-heme complex observed in the purified *Cb* H-NOX.[6] The reported K_D(NO) was thus an apparent value, $K_{D,apparent}$(NO) = k_{off}(5c NO-heme)/k_{on}(6c NO-heme-His). Since k_{off}(NO) of a 5c NO-heme complex is usually significantly smaller than that of a 6c NO-

heme-His complex (Table 1), the apparent $K_{D,apparent}$(NO) previously calculated is much smaller than the true K_D(NO) (reaction IV). Therefore, the previously reported value of K_D(NO) was greatly underestimated for *Cb* H-NOX. A similar case of misrepresenting the K_D(NO)(6c) of a hemoprotein with an apparent $K_{D,apparent}$(NO) was sGC.[3] In that case, k_{off} = 6 × 10^{-4} s^{-1}, for 5c NO-heme, was used to calculate a $K_{D,apparent}$(NO) = 4.2 × 10^{-12} M, which was misinterpreted as the K_D(NO) of sGC.[24,25] The K_D(NO)(6c) of sGC, 5.4 × 10^{-8} M, was later obtained by measuring the k_{off}(NO) of its 6c NO-sGC complex, 27 s^{-1}.[11] Combining the results from this and previous studies, it is now clear that *Cb* H-NOX binds NO with a K_D(NO) of 8.0 × 10^{-11} M (Table 1), which is comparable to the K_D(NO)'s of other bacterial H-NOXs. On the other hand, dissociation of NO from *Cb* H-NOX may significantly slow down due to essentially irreversible conversion of its initial 6c NO-heme-His complex to a 5c NO-heme complex.

The k_{off}(NO) of 5c NO-heme complex measured previously[6] is about 3 orders of magnitude slower than that measured in this study (Table 1). One possible reason for the extremely slow k_{off}(NO) measured previously is the inclusion of reducing agent, 15 mM β-mercaptoethanol (βME) in the buffer. βME effectively lowered the concentration of O_2, which served as the only scavenging reagent for dissociated NO, resulting in significant rebinding of NO and therefore very slow decay of EPR signal of NO-heme complex. The presence of 85–90% unliganded *Cb* H-NOX in the previous EPR sample[6] also slowed down the observed decay of the EPR signal. This portion of *Cb* H-NOX was present in the ferrous state when the protein was purified in the presence βME.[6] In the EPR measurement of k_{off}(NO), the reassociation of NO, which was present due to the lack of scavenger, with the unliganded ferrous *Cb* H-NOX may be prominent and led to further underestimation of the true k_{off}(5c NO-heme). Slow k_{off}(NO) of 5c NO-heme complex, lack of NO scavenger, and presence of prominent unliganded ferrous heme with open distal binding pocket collectively enabled the 5c NO-heme formed *in vivo* survive the purification in the previous study.[6] No EPR signal of NO-heme complex(es) was observed in the purified *Cb* H-NOX in this study. Since no reducing agent was used during purification, *Cb* H-NOX purified in this study was in its ferric state, confirmed by no further reaction after adding ferricyanide (data not shown). NO completely dissociated from ferric *Cb* H-NOX due to the much weaker affinity of NO for ferric heme than for ferrous heme. Another minor factor which further reduces k_{off}(NO) of the 5c NO-heme complex measured in the previous study was that the dissociation was monitored at relatively low temperature, 277 K,[6] about 20 degrees lower than the experimental temperature in this study.

O_2 Binding to *Cb* H-NOX.

In this study, it is clearly demonstrated that *Cb* H-NOX binds O_2 under normal atmospheric pressure, but no oxyferrous *Cb* H-NOX complex was previously observed.[6] One possible reason is that the auto-oxidation of oxyferrous *Cb* H-NOX is faster than that of *Tt* H-NOX. In fact, resting wt *Cb* H-NOX was purified in its ferric state, and resting wt *Tt* H-NOX was purified as an oxyferrous complex (Figure S5). However, since reducing reagent βME was included in the buffers for purifying wt *Cb* H-NOX previously,[6] a more plausible reason for not detecting any oxyferrous *Cb* H-NOX previously was that βME decreased [O_2] in the buffers to a level much lower than the $K_D(O_2)$ of *Cb* H-NOX.

In the crystal structure of *Tt* H-NOX complexed with O_2, the oxyferrous heme is stabilized by a network of hydrogen bonding including the primary interaction from the hydroxyl group of Y140 to O_2 and the secondary ones involving W9 and N74 to Y140, fixing the orientation of Y140. Such a hydrogen bonding network enhances the affinity of *Tt* H-NOX for O_2, confirmed because Y140F mutation eliminates O_2 binding in Y140F *Tt* H-NOX.[7,23] The distal heme pocket in *Cb* H-NOX is very similar to that in *Tt* H-NOX, revealed by structural comparison and sequence alignment between these two H-NOXs.[6] The similarities include (1) conservation of the key residues involved in hydrogen bond network in *Cb* H-NOX, namely, Y139, W9, and N73; (2) conservation of residues which define the polarity of distal heme pocket, L144, F78, and I5 in *Tt* H-NOX and L143, F77, and V5 in *Cb* H-NOX. The similarity of the binding pockets in *Cb* and *Tt* H-NOXs suggests that they have similar $k_{on}(O_2)$'s, and the oxyferrous complexes in both H-NOXs are stabilized by hydrogen bonding interactions through their distal tyrosine residues.[26] The importance of Y139 in stabilizing the oxyferrous complex in *Cb* H-NOX, just as Y140 in *Tt* H-NOX, is underscored by the undetection of oxyferrous complex in Y139F *Cb* and Y140F *Tt* H-NOXs.[23] On the other hand, despite the similarity of the distal heme pockets in *Cb* and *Tt* H-NOXs, their $K_D(O_2)$ constants exhibit a 3-order difference. The much larger $K_D(O_2)$ of *Cb* H-NOX is likely due to its very large $k_{off}(O_2)$, suggesting that the hydrogen bonding interactions for stabilizing the oxyferrous complex is weaker in *Cb* H-NOX compared to those in *Tt* H-NOX. Although *Cb* H-NOX is predicted to have similar distal hydrogen bonding constellation as *Tt* H-NOX, the unconserved residues around its heme pocket may introduce conformational flexibility which weakens distal hydrogen bonding leading to a less stable oxyferrous complex. A molecular dynamic simulation suggests that the dynamics of the protein conformation around the O_2 binding site is different in *Cb* and *Tt* H-NOXs, providing some insights into the difference between the $K_D(O_2)$'s of these two H-NOXs'.[27] On the other hand, such conformational flexibility is not expected to affect the bindings of CO and NO significantly based on the study showing that electrostatic hydrogen bonding donor at the distal heme pocket provides discriminative stabilization of 100:10:1 for O_2:NO:CO in Mb.[28] *Cb* H-NOX does exhibit K_D(CO) and K_D(NO) which are only slightly higher than those of *Tt* H-NOX. Although *Cb* H-NOX is capable of forming an oxyferrous complex under atmospheric pressure, its $K_D(O_2)$ is more than 600-fold higher than $[O_2]$ of the strict anaerobic conditions under which *C. botulinum* germinates, $[O_2] < 2$ ppm (or 8.2×10^{-8} M at 25 °C).[29] Therefore, obligate anaerobe *C. botulinum* unlikely depends on *Cb* H-NOX to sense the level of oxygen.

Contrary to its stabilizing effect for oxyferrous *Cb* H-NOX, distal Y139, seems to destabilize the Fe–His bond in the 6c NO-heme-His complex in *Cb* H-NOX, as less 6c NO-heme-His converts to 5c NO-heme complex in Y139F *Cb* H-NOX, indicated by both optical and EPR data (Figures 1 and 4). A more stable 6c NO-heme-His complex in Y139F *Cb* H-NOX was previously reported based on optical data[6] and substantiated by our EPR study (Figures 4 and 5). On the other hand, mutations of the corresponding distal tyrosine in *Tt* H-NOX, Y140L, and Y140F, do not affect the coordination number of NO complex as demonstrated in previous UV–vis optical study[20] and by our EPR data. Interestingly, F142Y mutation, which introduces a distal tyrosine into one of the H-NOXs from *Legionella pneumophila* (*L2* H-NOX), stabilizes its 6c NO-heme-His complex.[20] It is still not clear why distal tyrosine in

different H-NOXs have different effects on the stability of the Fe–His bond in their 6c NO-heme-His complexes, as DFT calculations suggest that hydrogen bond energy of a phenol group to NO is similar in both 5c and 6c heme-NO complexes.[30] Detailed resonance Raman spectroscopy studies on the NO complexes of *Cb* and *Tt* H-NOXs and their distal tyrosine to phenylalanine mutants are underway and may provide new insights into this issue. EPR evidence in this study further reveals that distal tyrosine may tune the heme geometry of the 6c NO-heme-His complex in an H-NOX. This is demonstrated by the decreased rhombicity of the 6c NO-heme-His complex in Y140F *Tt* H-NOX (Figure 5).

Supplementary Material

Refer to Web version on PubMed Central for supplementary material.

Funding

This work was supported by NIH Grant RO1 HL 095820 to A.-L.T.

ABBREVIATIONS

H-NOX	heme nitric oxide and oxygen binding protein
***Cb* H-NOX**	H-NOX from *Clostridium botulinum*
***L2* H-NOX**	H-NOX from *Legionella pneumophila*
***Ns* H-NOX**	H-NOX from *Nostoc punctiforme*
***Tt* H-NOX**	H-NOX from *Thermoanaerobacter tengcongensis*
***Vc* H-NOX**	H-NOX from *Vibrio cholera*
sGC	soluble guanylyl cyclase

REFERENCES

(1). Boon EM, and Marletta MA (2005) Ligand specificity of H-NOX domains: from sGC to bacterial NO sensors. J. Inorg. Biochem 99, 892–902. [PubMed: 15811506]

(2). Shimizu T, Huang D, Yan F, Stranava M, Bartosova M, Fojtikova V, and Martinkova M (2015) Gaseous O2, NO, and CO in signal transduction: structure and function relationships of heme-based gas sensors and heme-redox sensors. Chem. Rev 115, 6491–6533. [PubMed: 26021768]

(3). Tsai A-L, Martin E, Berka V, and Olson JS (2012) How do heme-protein sensors exclude oxygen? Lessons learned from cytochrome c', Nostoc puntiforme heme nitric oxide/oxygen-binding domain, and soluble guanylyl cyclase. Antioxid. Redox Signaling 17, 1246–1263.

(4). Derbyshire ER, and Marletta MA (2009) Biochemistry of soluble guanylate cyclase. Handb Exp Pharmacol 191, 17–31.

(5). Wu G, Liu W, Berka V, and Tsai A-L (2013) The Selectivity of Vibrio cholerae H-NOX for Gaseous Ligands Follows the ″Sliding Scale Rule″ Hypothesis. Ligand Interactions with both Ferrous and Ferric Vc H-NOX. Biochemistry 52, 9432–9446. [PubMed: 24351060]

(6). Nioche P, Berka V, Vipond J, Minton N, Tsai A-L, and Raman CS (2004) Femtomolar sensitivity of a NO sensor from Clostridium botulinum. Science 306, 1550–1553. [PubMed: 15472039]

(7). Pellicena P, Karow DS, Boon EM, Marletta MA, and Kuriyan J (2004) Crystal structure of an oxygen-binding heme domain related to soluble guanylate cyclases. Proc. Natl. Acad. Sci. U. S. A 101, 12854–12859. [PubMed: 15326296]

(8). Ma X, Sayed N, Beuve A, and van den Akker F (2007) NO and CO differentially activate soluble guanylyl cyclase via a heme pivot-bend mechanism. EMBO J. 26, 578–588. [PubMed: 17215864]

(9). Herzik MA Jr., Jonnalagadda R, Kuriyan J, and Marletta MA (2014) Structural insights into the role of iron-histidine bond cleavage in nitric oxide-induced activation of H-NOX gas sensor proteins. Proc. Natl. Acad. Sci. U. S. A 111, E4156–4164. [PubMed: 25253889]

(10). Erbil WK, Price MS, Wemmer DE, and Marletta MA (2009) A structural basis for H-NOX signaling in Shewanella oneidensis by trapping a histidine kinase inhibitory conformation. Proc. Natl. Acad. Sci. U. S. A 106, 19753–19760. [PubMed: 19918063]

(11). Tsai A-L, Berka V, Martin E, and Olson JS (2012) A ″sliding scale rule″ for selectivity among NO, CO, and O(2) by heme protein sensors. Biochemistry 51, 172–186. [PubMed: 22111978]

(12). Tsai A-L, Berka V, Martin F, Ma X, van den Akker F, Fabian M, and Olson JS (2010) Is Nostoc H-NOX a NO sensor or redox switch? Biochemistry 49, 6587–6599. [PubMed: 20572679]

(13). Brent RP (1973) Algorithms for Minimization without Derivatives, Prentice-Hall, Englewood Cliffs, NJ.

(14). Olson JS (1981) Stopped-flow, rapid mixing measurements of ligand binding to hemoglobin and red cells. Methods Enzymol. 76, 631–651. [PubMed: 7329281]

(15). Winter MB, Herzik MA Jr., Kuriyan J, and Marletta MA (2011) Tunnels modulate ligand flux in a heme nitric oxide/oxygen binding (H-NOX) domain. Proc. Natl. Acad. Sci. U. S. A 108, E881–889. [PubMed: 21997213]

(16). Martin E, Berka V, Tsai A-L, and Murad F (2005) Soluble guanylyl cyclase: the nitric oxide receptor. Methods Enzymol. 396, 478–492. [PubMed: 16291255]

(17). Andrew CR, George SJ, Lawson DM, and Eady RR (2002) Six- to five-coordinate heme-nitrosyl conversion in cytochrome c' and its relevance to guanylate cyclase. Biochemistry 41, 2353–2360. [PubMed: 11841228]

(18). Tsai A-L, Berka V, Sharina I, and Martin E (2011) Dynamic ligand exchange in soluble guanylyl cyclase (sGC): implications for sGC regulation and desensitization. J. Biol. Chem 286, 43182–43192. [PubMed: 22009742]

(19). Boon EM, Davis JH, Tran R, Karow DS, Huang SH, Pan D, Miazgowicz MM, Mathies RA, and Marletta MA (2006) Nitric oxide binding to prokaryotic homologs of the soluble guanylate cyclase beta1 H-NOX domain. J. Biol. Chem 281, 21892–21902. [PubMed: 16728401]

(20). Boon EM, Huang SH, and Marletta MA (2005) A molecular basis for NO selectivity in soluble guanylate cyclase. Nat. Chem. Biol 1, 53–59. [PubMed: 16407994]

(21). Karow DS, Pan D, Tran R, Pellicena P, Presley A, Mathies RA, and Marletta MA (2004) Spectroscopic characterization of the soluble guanylate cyclase-like heme domains from Vibrio cholerae and Thermoanaerobacter tengcongensis. Biochemistry 43, 10203–10211. [PubMed: 15287748]

(22). Weinert EE, Phillips-Piro CM, Tran R, Mathies RA, and Marletta MA (2011) Controlling conformational flexibility of an O_2-binding H-NOX domain. Biochemistry 50, 6832–6840. [PubMed: 21721586]

(23). Boon EM, and Marletta MA (2006) Sensitive and selective detection of nitric oxide using an H-NOX domain. J. Am. Chem. Soc 128, 10022–10023. [PubMed: 16881625]

(24). Zhao Y, Brandish PE, Ballou DP, and Marletta MA (1999) A molecular basis for nitric oxide sensing by soluble guanylate cyclase. Proc. Natl. Acad. Sci. U. S. A 96, 14753–14758. [PubMed: 10611285]

(25). Kharitonov VG, Russwurm M, Magde D, Sharma VS, and Koesling D (1997) Dissociation of nitric oxide from soluble guanylate cyclase. Biochem. Biophys. Res. Commun 239, 284–286. [PubMed: 9345311]

(26). Springer BA, Sligar SG, Olson JS, and Phillips GN Jr. (1994) Mechanisms of Ligand Recognition in Myoglobin. Chem. Rev 94, 699–714.

(27). Menyhard DK (2011) Conformational selection mechanism governs oxygen ligation to H-NOX proteins. Bioorg. Med. Chem. Lett 21, 3523–3526. [PubMed: 21602045]

(28). Olson JS, and Phillips GN Jr. (1997) Myoglobin discriminates between O2, NO, and CO by electrostatic interactions with the bound ligand. J. Biol. Inorg. Chem 2, 544–552.

(29). Young-Perkins KE, and Merson RL (1987) *Clostridium botulinum* spore germination, outgrowth, and toxin production below 4.6; interactions between pH, total acidity, and buffering capacity. J. Food Sci 52, 1084–1088.

(30). Tangen E, Svadberg A, and Ghosh A (2005) Toward modeling H-NOX domains: a DFT study of heme-NO complexes as hydrogen bond acceptors. Inorg. Chem 44, 7802–7805. [PubMed: 16241129]

(31). Yoo BK, Lamarre I, Rappaport F, Nioche P, Raman CS, Martin JL, and Negrerie M (2012) Picosecond to second dynamics reveals a structural transition in Clostridium botulinum NO-sensor triggered by the activator BAY-41–2272. ACS Chem. Biol 7, 2046–2054. [PubMed: 23009307]

(32). Martin E, Berka V, Sharina I, and Tsai A-L (2012) Mechanism of binding of NO to soluble guanylyl cyclase: implication for the second NO binding to the heme proximal site. Biochemistry 51, 2737–2746. [PubMed: 22401134]

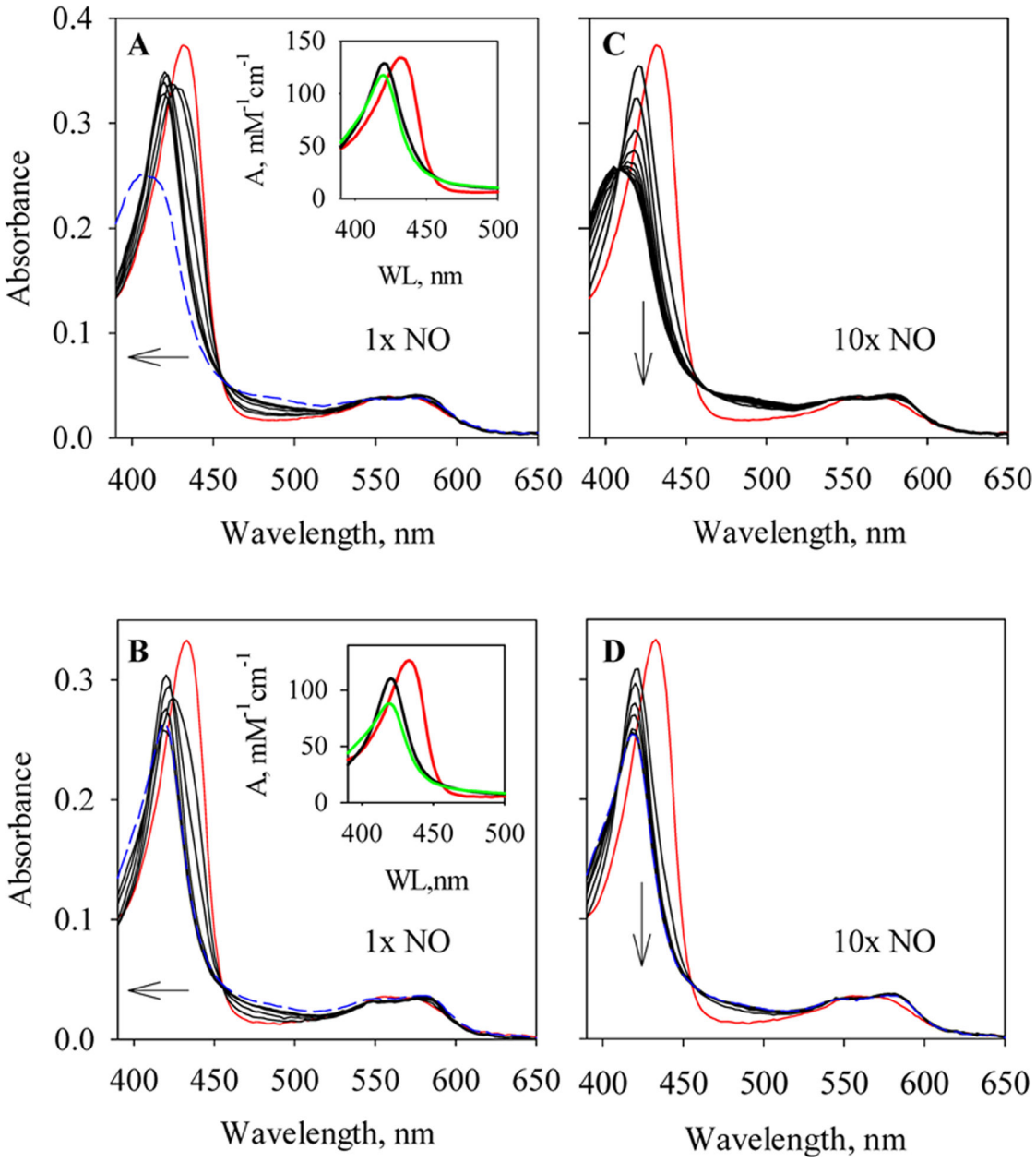

Figure 1.

Rapid-scan of NO binding to wt and Y139F *Cb* H-NOXs. (A) Reaction of 3.3 μM wt *Cb* H-NOX with 1 equiv of NO monitored for 0.3 s (black). Spectra at selected time points, 1.28, 3.84, 11.5, 49.9, 152.3, and 254.7 ms, are presented. The spectrum of wt *Cb* H-NOX mixed with anaerobic buffer (red) represents the spectrum at 0 s of the reaction. The Soret peak shifts from 432 to 420 nm; and further shifts to 409 nm after 6 s (blue dashed). Inset. The Soret region of the two intermediates resolved from the 0.3 s reaction, *B* (black) and *C* (green), based on model $A \rightarrow B \rightarrow C$, are plotted together with that of ferrous wt *Cb* H-NOX (*A*, red). (B) Reaction of 3.4 μM Y139F *Cb* H-NOX with 1 equiv NO monitored for 0.3 s (black). Spectra at selected time points, 1.28, 3.84, 24.3, 126.7, and 254.7 ms, are presented. The spectrum of Y139F *Cb* H-NOX mixed with anaerobic buffer (red) represents

the spectrum at 0 s of the reaction. The Soret peak shifts from 432 to 420 nm, and does not shift further up to 524 s (blue dashed). Inset. The Soret region of the two optically resolved intermediates from the 0.3 s reaction, *B* (black) and *C* (green), based on model $A \rightarrow B \rightarrow C$, are plotted together with that of ferrous Y139F *Cb* H-NOX (*A*, red). (C) Reaction of 3.3 μM wt *Cb* H-NOX with 10 equiv of NO monitored for 0.3 s (black). Spectra at selected time points, 1.28, 11.5, 24.3, 37.1, 49.9, 62.7, 75.5, 101.1, 152.3, 203.5, and 254.7 ms, are presented. Red line, same as in (A). The Soret peak shifts from 432 to 409 nm. (D) Reaction of 3.4 μM Y139F *Cb* H-NOX with 10 equiv NO monitored for 0.3 s (black). Spectra at selected time points, 1.28, 11.5, 24.3, 37.1, 75.5, 126.7, and 254.7 ms, are presented. Red line, same as in (B). The Soret peak shifts from 432 to 420 nm without any further shift after 524 s (blue dashed). The arrows indicate the directions of spectral changes.

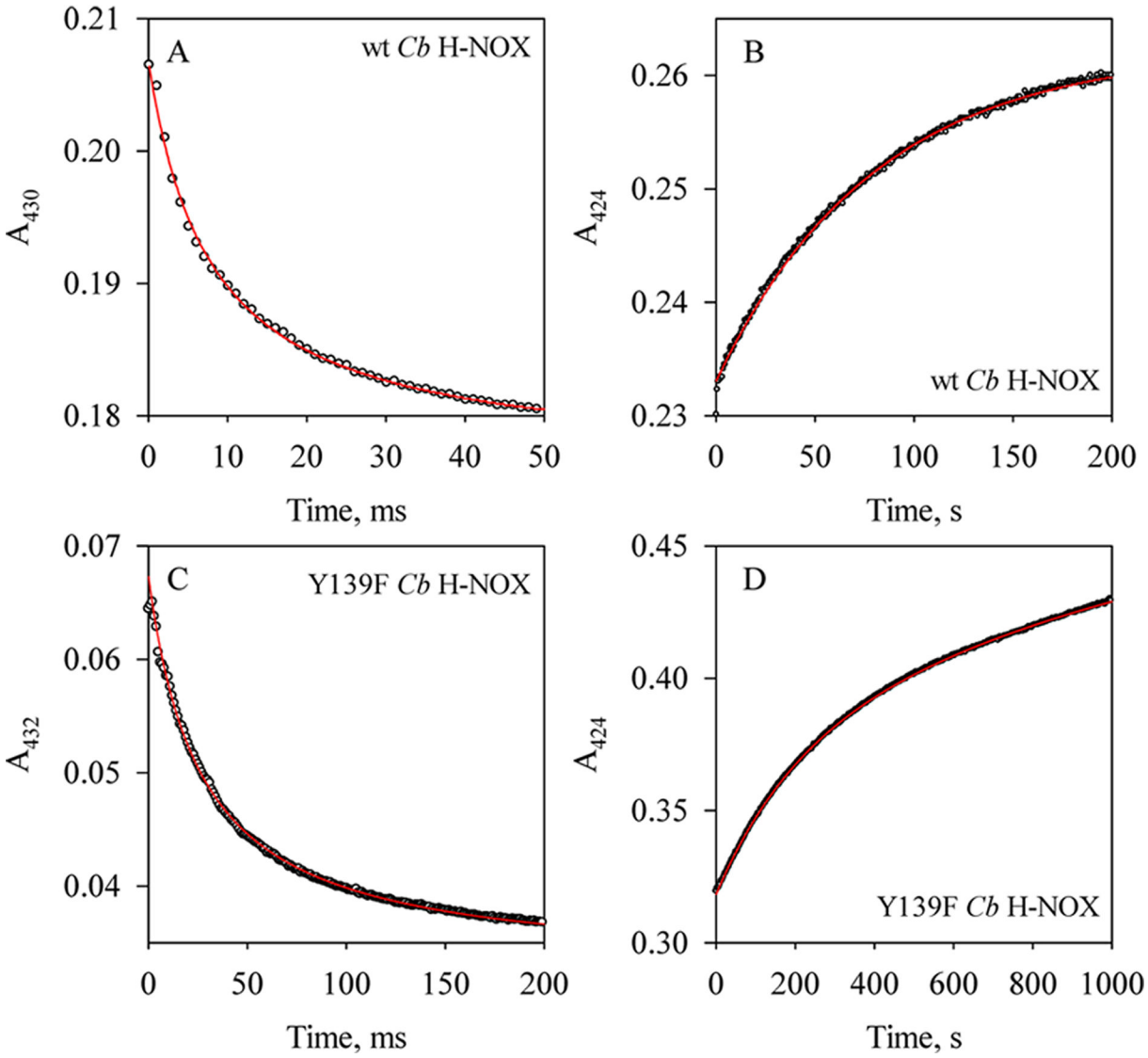

Figure 2.

Kinetics of the formation/dissociation of 6c NO complexes of wt and Y139F *Cb* H-NOXs. (A) Time course of A_{430} during the reaction of 2.3 μM wt *Cb* H-NOX with 1 equiv of NO (circles) and its fit to the eq 3 (red line). (B) Time course of A_{424} during the sequential stopped-flow reaction, 2.3 μM wt *Cb* H-NOX was first reacted with 1 equiv of NO, aged for 100 ms and then reacted with 50 mM dithionite with 1 mM CO (circles), and fitting to equation $A = A_{\max} \times \left(1 - e^{-k_{\text{obs}}t}\right)$ (red line), where $A_{\max}$ is the maximal level of A_{424} and t is the reaction time. (C) Time course of A_{432} during the reaction of 0.5 μM Y139F *Cb* H-NOX with 1 equiv of NO (circles), and k_{obs} obtained by fitting to eq 3 (red line). (D) Time course of A_{424} during the reaction of 3.0 μM Y139F *Cb* H-NOX with 1 equiv of NO then reacted with 50 mM dithionite with 1 mM CO (circles), and k_{obs} obtained by fitting to the same equation as in (B) (red line).

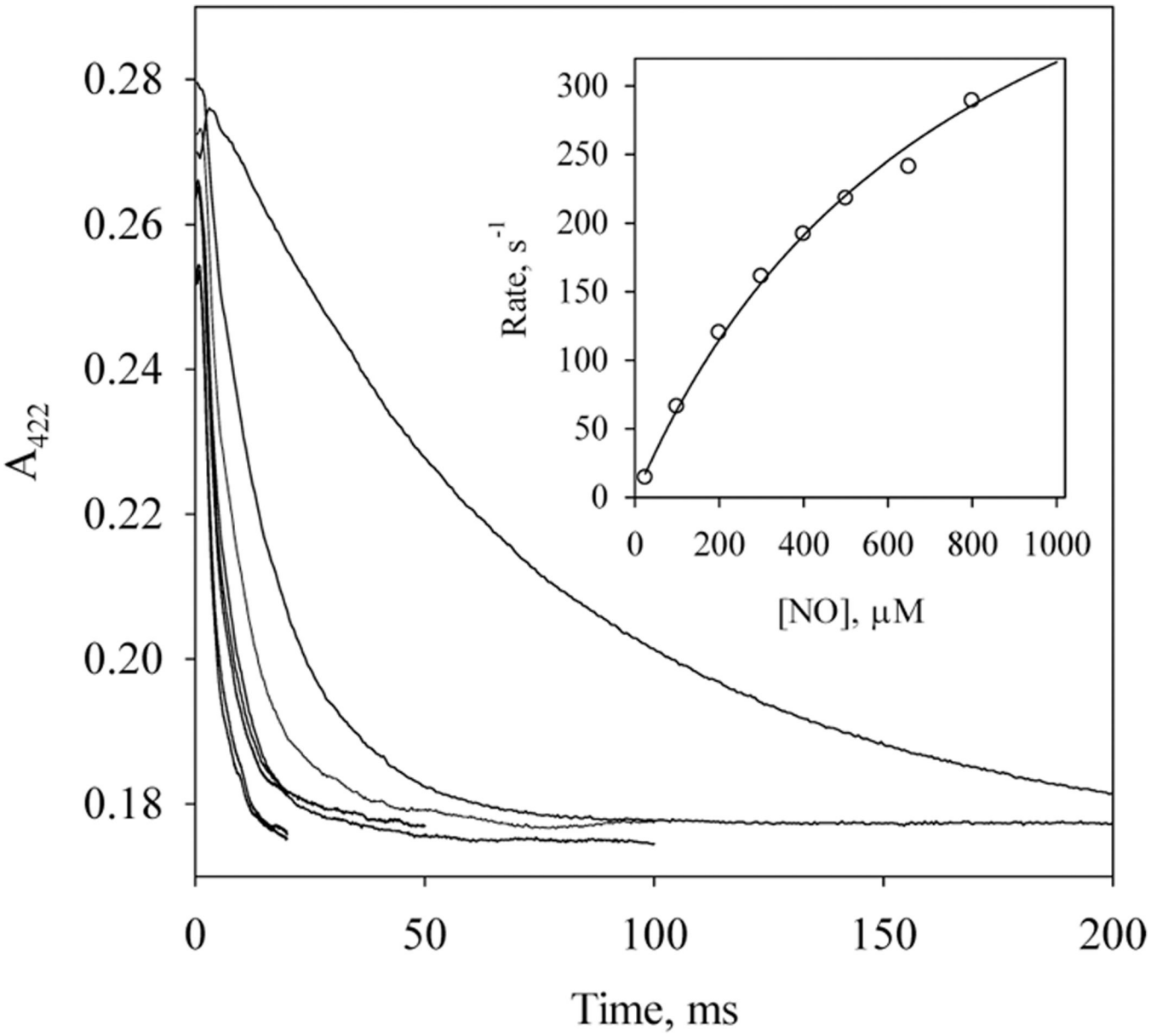

Figure 3.

Saturation kinetics for the reaction of wt *Cb* H-NOX with excess NO. Time courses of A_{422} during the reactions of 2.3 μM *Cb* H-NOX with 25, 100, 200, 300, 400, 500, 650, 800, and 1000 μM NO (from top to bottom, respectively) at 24 °C. Inset. Dependence of observed rate constants, k_{obs} (○) on [NO] and its fit to eq 5 (line).

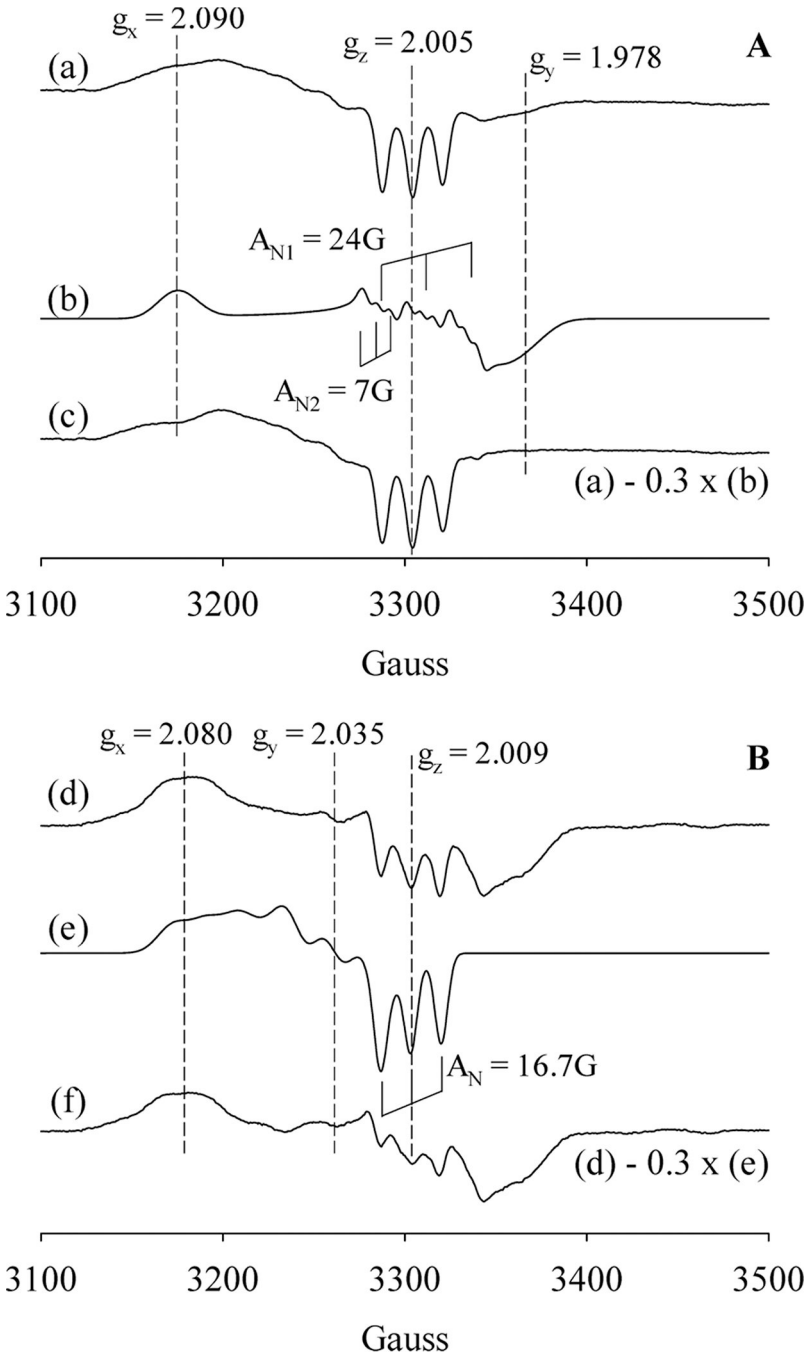

Figure 4.

EPR of wt and Y139F *Cb* H-NOXs with excess NO. Panel A. (a) Reaction of 4.5 μM wt *Cb* H-NOX with 20 equiv of NO for 1 min, exhibiting EPR signatures of the majority a 5c NO-heme complex plus a minor portion of a 6c NO-heme-His complex. (b) EPR spectrum of a 6c NO-heme-His complex simulated using the following parameters: g_x = 2.090, g_y = 1.978, g_z = 2.005; A_{N1}: A_x = 6 G; A_y = 10 G and A_z = 24.0 G; A_{N2}: A_x = 6 G; A_y = 10 G and A_z = 7 G. (c) Subtraction of 30% of (b) from (a) yields an EPR spectrum of a pure 5c NO-heme complex. Panel B. (d) Reaction of 6.0 μM Y139F *Cb* H-NOX reacted with 20 equiv NO for

1 min, exhibiting EPR signatures of the majority a 6c NO-heme-His complex with a minor portion of a 5c NO-heme complex. (e) EPR spectrum of a 5c NO-heme complex simulated using the following parameters: $g_x = 2.080$, $g_y = 2.035$, $g_z = 2.009$; A_N: $A_x = 18$ G; $A_y = 20$ G and $A_z = 16.7$ G. (f) Subtraction of 30% of (e) from (d) yields an EPR spectrum of a pure 6c NO-heme-His complex.

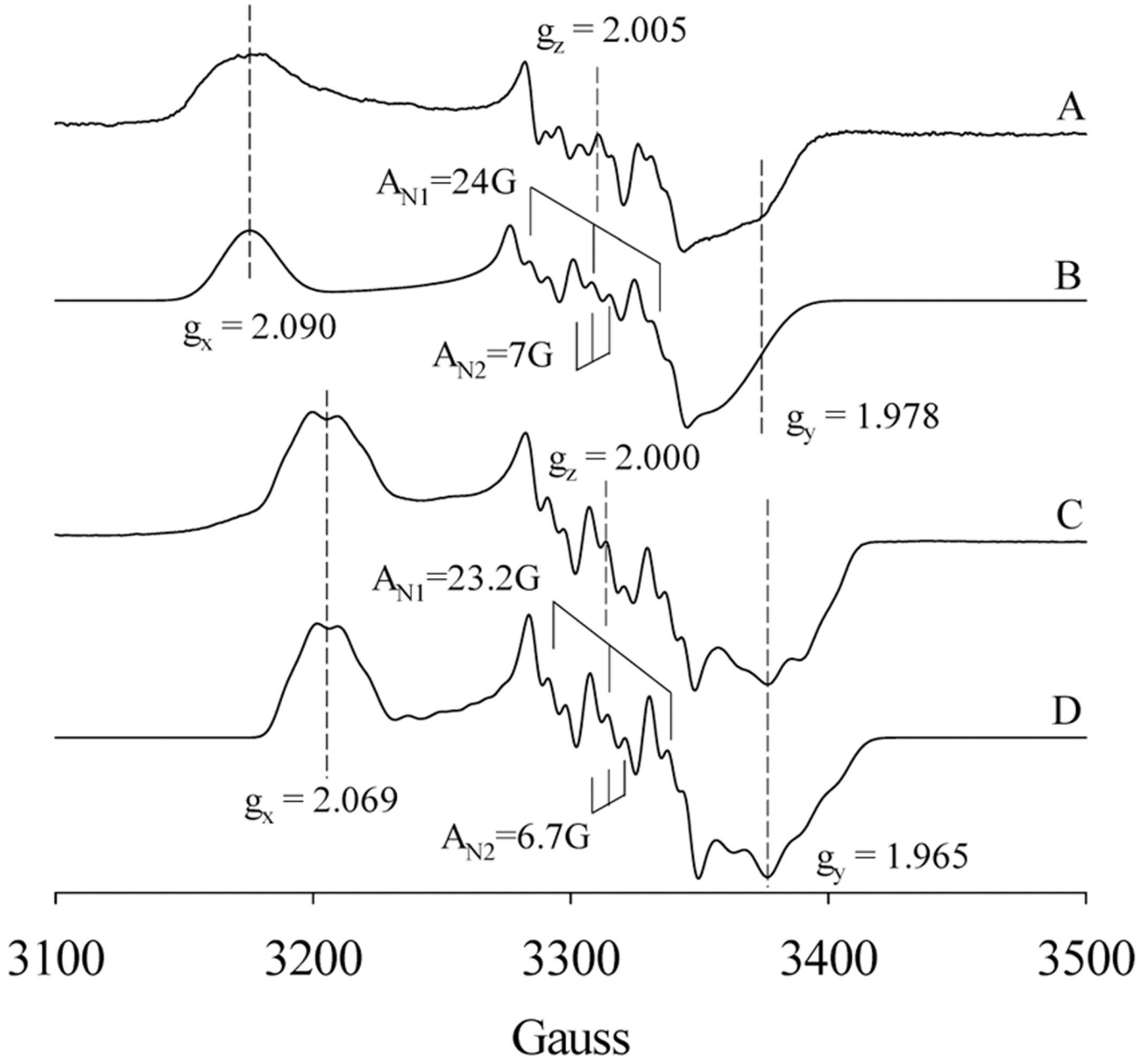

Figure 5.

EPR of wt and Y140F *Tt* H-NOXs with excess NO. (A) NO-heme-His complex trapped after 13 μM wt *Tt* H-NOX reaction with 30 equiv of NO for 1 min. (B) Simulation of the EPR spectrum A using the following parameters: g_x = 2.090, g_y = 1.978, g_z = 2.005; A_{N1}: A_x = 6 G; A_y = 10 G and A_z = 24.0 G; A_{N2}: A_x = 6 G; A_y = 10 G and A_z = 7 G. (C) NO-heme-His complex trapped after 95 μM Y140F *Tt* H-NOX reaction with 5 equiv of NO for 1 min. (D) Simulation of the EPR spectrum C using the following parameters: g_x = 2.069, g_y = 1.965, g_z = 2.000; A_{N1}: A_x = 10 G; A_y = 13 G, and A_z = 22.2 G; A_{N2}: A_x = 6 G; A_y = 13 G, and A_z = 6.7 G.

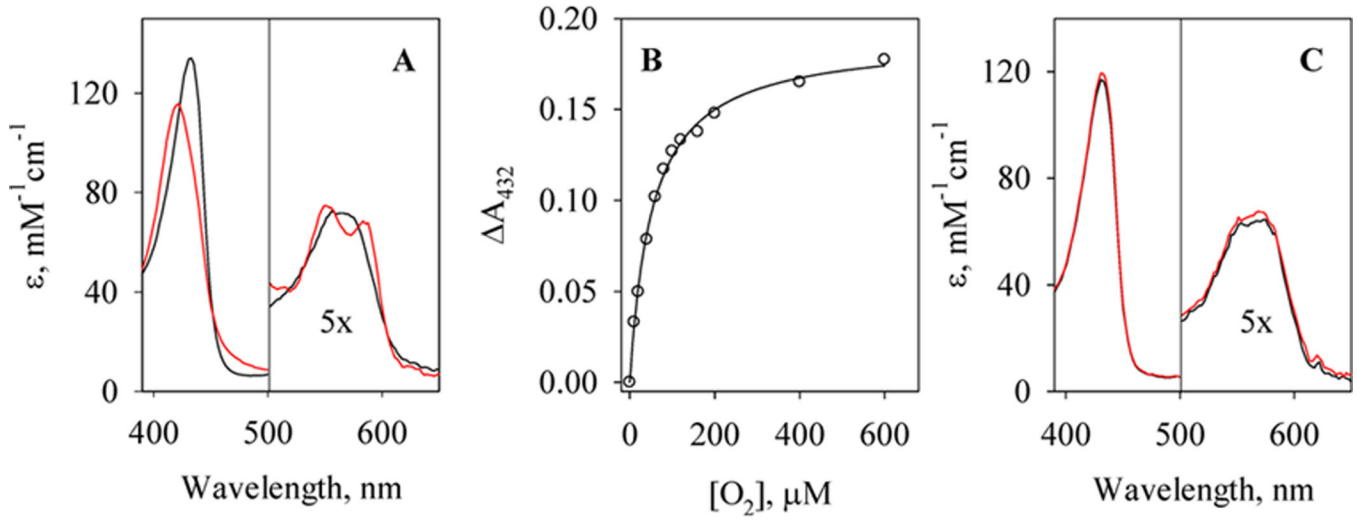

Figure 6.

Interaction of O_2 with wt and Y139F *Cb* H-NOXs. (A) Spectra of 3.6 μM anaerobic ferrous *Cb* H-NOX (black) and the first spectrum of rapid-scan reaction with aerobic buffers (red), $[O_2]_{final} \approx 120$ μM. The *y*-axis represents the extinction coefficients. (B) The change of A_{432}, the Soret of *Cb* H-NOX, in the reaction of 3.3 μM *Cb* H-NOX with various concentrations of O_2 (circle) and its fit using eq 6 (solid line). (C) Spectra of 2.2 μM anaerobic Y139F *Cb* H-NOX before (black) and after (red) mixing with O_2-saturated buffer, $[O_2]_{final} \approx 600$ μM. The *y*-axis represents the extinction coefficients.

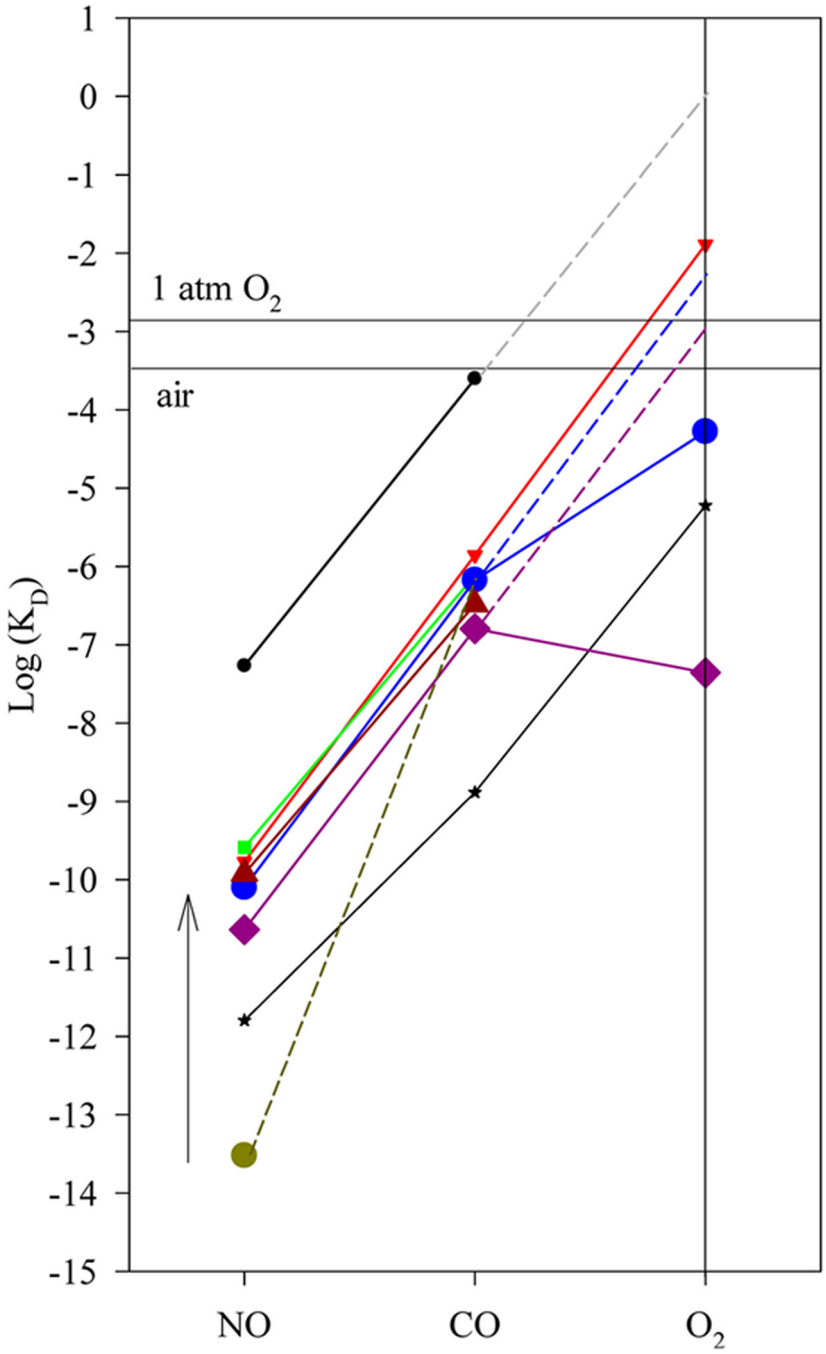

Figure 7.

Relationship of log K_D's for H-NOXs versus ligand type. The measured logarithm values of K_D(NO), K_D(CO), and K_D(O_2) of H-NOXs are plotted versus ligand type. K_D's measured for sGC and heme model ferrous PPIX(1-MeIm) are also plotted for comparisons. Wt *Cb* H-NOX (blue circle); Y139F *Cb* H-NOX (brown triangle); *Tt* H-NOX (purple diamond); *Vc* H-NOX (green square); *Ns* H-NOX (red triangle); sGC (black circle) (an extrapolation from sGC log K_D(NO)-log K_D(CO) line, gray dashed line, predicts its K_D(O_2) ≈ 1.1 M) and ferrous PPIX (1-MeIm) (black star). The K_D(NO) (dark yellow circle) of *Cb* H-NOX

previously measured[6] is connected to its K_D(CO) by the broken line; the change between the K_D(NO) measured in this study, and the previously measured value is represented by the arrow. The blue and purple dashed lines represent the prediction of $K_D(O_2)$'s of *Cb* and *Tt* H-NOXs, respectively, based on the extrapolation from their log K_D(NO)-log K_D(CO) lines.

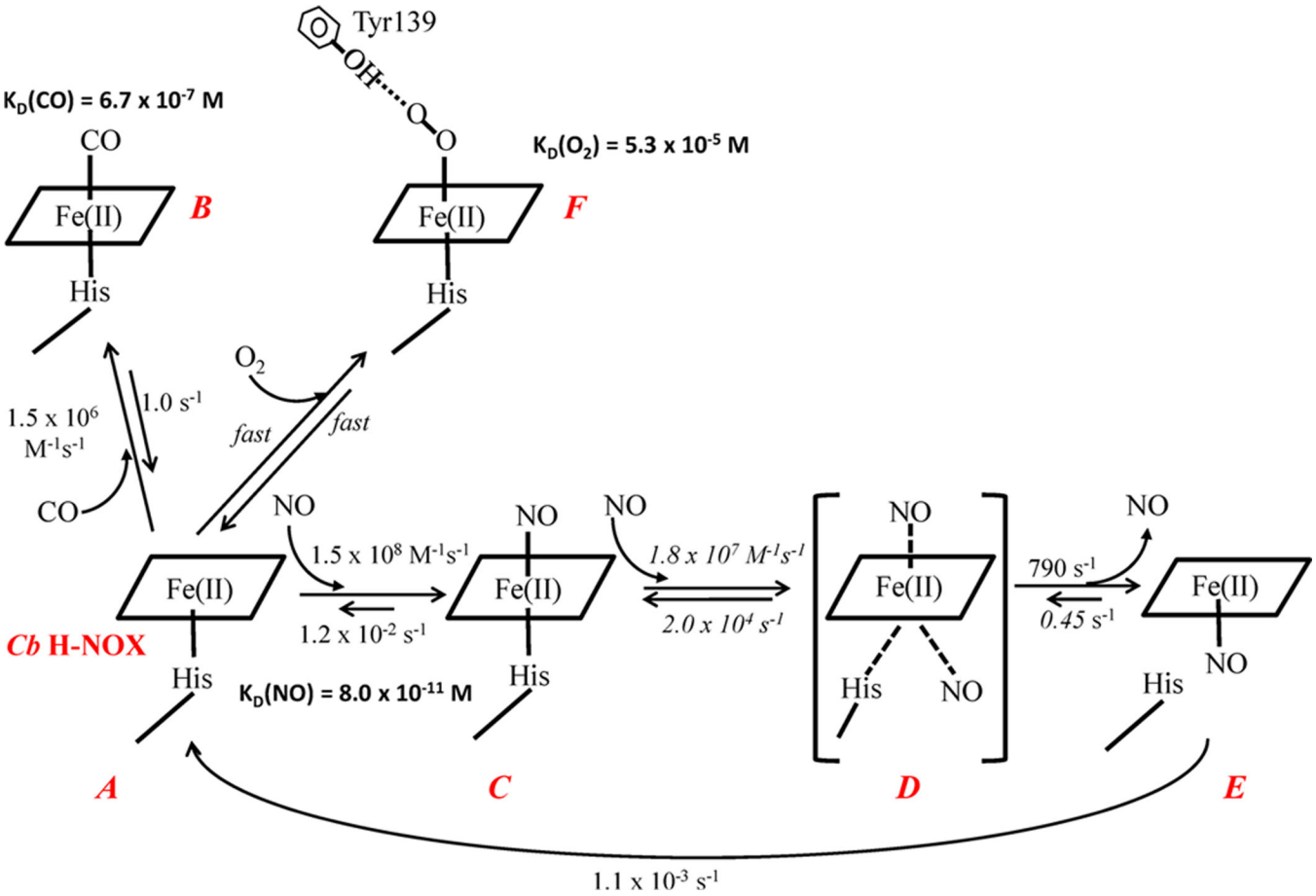

Scheme 1. Binding of Gaseous Ligands to Ferrous *Cb* H-NOX[a]

[a]Each heme species is labeled in red. The rate constants labeled in italic are estimated by computer modeling. Both association and dissociation of O_2 to ferrous *Cb* H-NOX (*A*) are assumed to be fast, and the rate constants are not determined, although $K_D(O_2)$ of *Cb* H-NOX was measured by stopped-flow titration method. $K_D(NO)$ is the affinity for 6c NO-heme-His complex. The putative hydrogen bonding from the hydroxyl group of Y139 to O_2-heme is represented by a dashed line. Intermediate *D*, bracketed in parentheses, is a quaternary complex as proposed before[32] and is not observed in experiment, for its extreme transient nature.

Table 1.

Gas Ligand Binding Parameters: k_{on}, k_{off}, and K_D of *Cb* and *Tt* H-NOXs, in Comparisons with Published Values

	O_2			CO			NO		
H-NOX	**k_{on} (M^{-1} s^{-1})**	**k_{off} (s^{-1})**	**K_D (M)**	**k_{on} (M^{-1} s^{-1})**	**k_{off} (s^{-1})**	**K_D (M)**	**k_{on} (M^{-1} s^{-1})**	**k_{off} (s^{-1})**	**K_D (M)**
wt *Cb*		~2500[b]	5.3×10^{-5}	1.5×10^{6}	1.0	6.7×10^{-7}	1.5×10^{8}	1.2×10^{-2}	8.0×10^{-11}
								1.1×10^{-3}[a]	
				1.5×10^{6}[d]			~ 10^{8}[c]	3×10^{-6}[c]	3.0×10^{-14}[c]
Y139F *Cb*				3.4×10^{6}	1.1	3.3×10^{-7}	4.3×10^{7}	5.0×10^{-3}	1.2×10^{-10}
wt *Tt*	4.3×10^{7}	1.9	4.4×10^{-8}	3.3×10^{6}	0.5	1.6×10^{-7}	1.5×10^{8}	3.4×10^{-3}	2.3×10^{-11}
	1.36×10^{7}[e]	1.2[e]	8.97×10^{-8}[e]	2.18×10^{6}[g]	3.56[g]	1.63×10^{-6}		5.6×10^{-4}	
	2.5×10^{7}[f]	1.2[f]	4.8×10^{-8}[f]	4.1×10^{6}[g]					

[a] k_{off} of 5c NO-heme complex.

[b] Estimated value.

[c] Ref 6.

[d] Ref 31.

[e] Ref 20.

[f] Ref 22.

[g] Ref 15.

K_D was calculated as ratio of k_{off} and k_{on} measured using stopped-flow method.

[h] Ref 19.